# 5B.4 State of the art in optimal control of series hybrid electric vehicles taking account of driveability

Conny Tempelhahn, Stephan Uebel, Bernard Bäker

## Abstract

This paper presents an energy management strategy, which is based on the optimal control theory, for series hybrid electric vehicles driving on fixed routes. The method presented combines deterministic dynamic programming and Pontryagin's maximum principle with the objective to minimise the fuel consumption. A comparison to the results which are obtained by dynamic programming indicates that the method presented is close to optimal. Moreover, this paper investigates driveability of the energy management strategy in terms of drivetrain activity, i.e. the amount and frequency of engine start events. Therefore, penalty costs are incorporated into the objective function to take the additional energy consumption when the diesel engine is started into account. The trade-off between fuel consumption and drivetrain activity is investigated by means of a sensitivity analysis of the engine start costs. Thus, numerous driving cycles, which have been extracted from real-world driving data of a specific bus line, are simulated. The study reveals that drivetrain activity can be significantly improved by manipulating the penalty costs.

## Kurzfassung

Dieser Beitrag stellt eine auf der Theorie der optimalen Steuerung basierende Methode zum Energiemanagement von seriellen Hybridfahrzeugen auf feststehenden Routen vor. Die vorgestellte Methode kombiniert die dynamische Programmierung mit Pontrjagins Maximumprinzip und hat zum Ziel, den Kraftstoffverbrauch zu minimieren. Ein Vergleich mit den Ergebnissen einer dynamischen Programmierung legt nahe, dass die vorgestellte Methode nahezu optimale Resultate liefert. Außerdem untersucht dieser Beitrag die Fahrbarkeit des Energiemanagements im Sinne der Antriebsstrangaktivität, das heißt die Anzahl und Häufigkeit der Motorstarts. Zu diesem Zweck wurde die Zielfunktion um Motorstartkosten erweitert, die den zusätzlichen Energieverbrauch zum Starten des Dieselmotors berücksichtigen. Der Zielkonflikt zwischen dem Kraftstoffverbrauch und der Antriebsstrangaktivität wird in Form einer Sensitivitätsanalyse der Motorstartkosten untersucht. Dafür wird eine Vielzahl von Fahrprofilen, welche aus realen Fahrdaten auf einer bestimmten Buslinie abgeleitet wurden, simuliert. Die Analyse zeigt, dass die Antriebsstrangaktivität durch Manipulation der Startkosten deutlich verbessert werden kann.

# 1. Introduction

Hybrid electric vehicles (HEVs) have the capability to save fuel and reduce pollutant emissions. Due to their additional energy storage along with an electric motor, HEVs are capable to recover braking energy. Furthermore, the resulting freedom to decide when to use which storage makes superior operational efficiency compared to conventional cars possible [18]. For parallel HEVs, the freedom of choosing the gear is very important as well in that context. Moreover, the internal combustion engine can be turned off, because most HEVs can be driven purely electrically. These freedoms are controlled by the so-called energy management strategy (EMS) which is also referred to as (supervisory) control strategy. The design of EMS strongly affects fuel consumption and driveability. Since both of them are crucial aspects when purchasing a vehicle, manufacturers pay considerable attention to them during the design process [22].
During the last two decades, researchers have put a lot of effort on developing different kinds of EMSs mainly focusing on fuel economy. A comprehensive overview of EMSs and recent publications can be found for example in [11], [17] and [24]. From that it can be seen that EMSs are commonly classified into *optimisation-based* and *rule-based* strategies [10], [24], [26], [34]. This classification (see Figure 1) developed due to the historic evolution of EMS because early controllers were mostly based on heuristic considerations of the designing engineer [28]. For instance, operating the combustion engine with low efficiency is avoided by running purely electrically. Unfortunately, both their design and parameterization strongly depend on the particular vehicle and the utilised driving cycles. Since a specific control objective cannot usually be pursued, rule-based strategies require considerable calibration. This means that their parameterisation has to be tuned to meet a specific objective such as fuel consumption. As a consequence, performance can be poor under certain driving conditions which have not been subject to the calibration [28]. These drawbacks spurred the endeavour to develop alternative EMSs using mathematical optimisation.

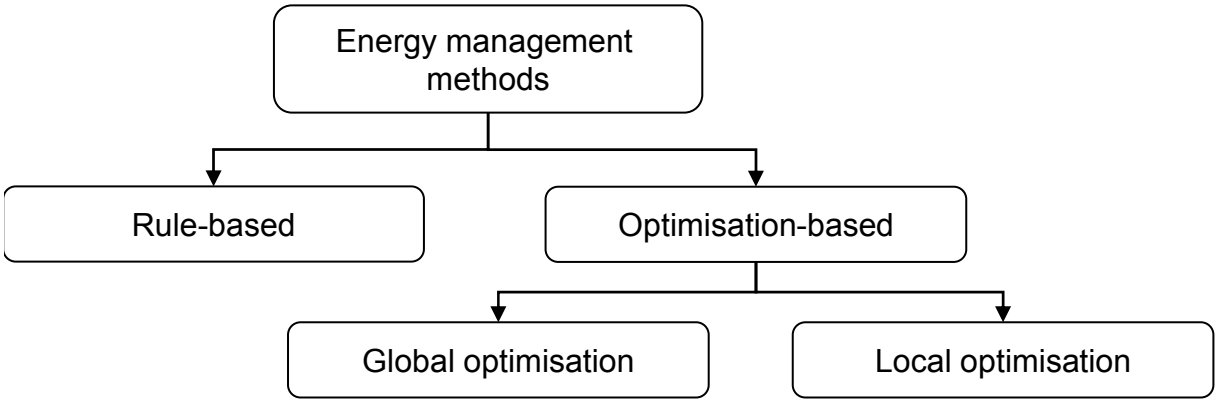


*Figure 1: Common classification of EMSs into rule-based and optimisation-based strategies. Global optimisation is necessary to determine the optimal solution.*

In general, optimisation-based EMSs minimise a specific objective function such as fuel consumption along a given horizon by controlling the freedoms of the system. To get a better grasp of the solution accuracy, optimisation-based EMSs can be separated into *local* and *global optimisation* [29]. This classification does not strictly specify the mathematical method but rather the manner of solving the optimisation problem. On the one hand, global optimisation considers the complete optimisation problem as a whole [29] yielding the optimal EMS. As a consequence, global optimisation

requires perfect knowledge of upcoming driving conditions, which means the driving cycle. However, this is not always possible in reality for the following reasons. Firstly, the route might not be known to the EMS. This obstacle can be overcome in scenarios with repeating driving conditions such as commuting where the route can be recognized using former trip data [9], [30]. Secondly, even if the route is known, predictive data will be uncertain due to disturbances through the driver and surrounding traffic. Thus, global optimisation is usually limited to *offline* usage, for example, to benchmark real-time capable EMSs or to deduce general design recommendations for EMSs. On the other hand, *local optimisation* reduces the global problem to sequences of local problems [29] yielding sub-optimal EMSs, at best. Such EMSs are usually suitable for *online* usage in real HEVs, for example by means of model predictive control (MPC) as shown in [13], [15], [20].

Many methods used in EMSs are based on optimal control theory which deals with deriving optimal control policies through minimisation of a mathematical optimization problem. Optimal control of HEVs normally yields mixed-integer optimisation problems because of inherently discrete decision variables such as gear position and engine state. Therefore, dynamic programming (DP) is widely used [12], [15], [19], [28], [29], [31], [35] since it is applicable to solve even non-convex and mixed-integer optimisation problems with constraints on control and state variables [8], [20]. However, DP is limited to problems with few state variables because computational burden increases exponentially with growing complexity, which is called the curse of dimensionality [2]. Pontryagin's maximum principle (PMP) is an alternative method for optimal control of HEVs [1], [14], [27], [28], [29]. EMSs based on PMP have been shown to obtain optimal results with significantly less computational effort than DP [20], [29]. With regard to computational effort, convex optimisation [5] is another even more efficient method that is applicable for optimal control of HEVs [21], too. However, the optimisation problem usually has to be turned into convex form manually, which requires further simplifications of the models. The major drawback of convex optimisation and PMP is that both methods cannot be applied to solve mixed-integer problems. Thus, discrete system states can only be considered as decision variables or have to be handled alternatively.

As a consequence, combinations of different methods have been proposed to circumvent the individual drawbacks while benefitting from the advantages [7], [16], [18], [19], [20], [21]. For example, the author of [20] decoupled the mixed-integer problem of a parallel hybrid drivetrain. The continuous sub-problem, i.e. the optimal power split, is solved in an inner loop using PMP without state constraints. Meanwhile, the discrete sub-problem, i.e. the gear position and engine state, is solved using DP in an outer loop. A similar approach has been proposed in [21], where convex optimisation is used instead of PMP. This approach can handle state constraints in contrast to the previous. Additionally, the author of [20] proposes to implement the introduced approach in a classical MPC scheme. A different MPC scheme with two decoupled control layers using PMP is proposed in [16]. The high level controller is realized as iterative PMP-based algorithm to determine the optimal costate for the low level controller which is in direct control of the drivetrain. The low level controller is realized as Equivalent Consumption Minimisation Strategy (ECMS) [23] which is closely related to PMP as shown in [31]. Another different MPC approach using former driving data by means of a stochastic model is proposed in [13]. This approach uses stochastic dynamic programming [4] to obtain online-capable controllers. However, most of the research in the field of energy management of HEVs is focused on

minimising fuel consumption or pollutant emission rather than paying attention to driveability.

The aspect of driveability has been encountered by the authors of the following publications [19], [21], [22], [25], [32], [35]. According to [22], driveability in general means the driver's perception of vehicle response and behaviour. This can include performance aspects like acceleration, engine noise, shifting activity and other dynamic behaviours such as driveline dynamics [25], [33]. Some of the aforementioned aspects are directly influenced by the EMS, e.g. gear shifting, changing the engine state, and the engine's operating point which affects engine noise. These aspects are called drivetrain activity hereinafter. Unfortunately, optimisation-based EMS will possibly cause high drivetrain activity if this is not penalised in the objective function. Therefore, most of the aforementioned approaches try to avoid frequent drivetrain activity by adding penalty costs for gear changes or engine events to the objective function. While most of the authors merely investigate the impact on optimal control and the resulting fuel consumption, only [22] and [32] actually investigate the trade-off between driveability and fuel consumption for a parallel HEV. The authors of [22] and [32] utilised stochastic dynamic programming and ECMS, respectively. However, since both methods are local optimization, they do not yield optimal results.

Therefore, this paper presents a fast EMS for series hybrid vehicles using optimal control. The so-called PMP-DP method is a combination of PMP and DP extending the ideas of [16] and [20]. Thereby, PMP is applied in order to determine the continuous optimal power split while the discrete decision variable, which decides between starting or stopping the EGU, is determined by DP. In addition, the method ensures state constraints and incorporates engine start costs into the objective function which makes improving driveability in terms of drivetrain activity possible. Another contribution of this paper is the investigation of the trade-off between fuel consumption and drivetrain activity. Therefore, numerous simulations using real-world driving data have been performed for various engine start costs. Although not presented in this paper, the PMP-DP method is suitable for online control of HEVs through implementation in a MPC scheme which uses ECMS as low level controller as proposed in [16].

The paper is outlined as follows. Section 2 gives a brief introduction into optimal control and describes the driving cycles and the vehicle model. Based on that, the optimal control problem is formulated. Section 3 introduces a holistic dynamic programming which is used to determine the baseline solution of the optimal control problem. In Section 4, the proposed PMP-DP approach is presented and validated using the baseline solution. Furthermore, a method to convert electric into equivalent fuel energy, which allows compensation of deviations from the final state constraints, is introduced. The detailed investigation of the trade-off between fuel consumption and drivetrain activity is provided in the 5$^{th}$ section. Section 6 concludes on the contents shown in this paper and gives some future directions.

## 2. Formulation of the optimal control problem

Before the optimisation problem is formulated, optimisation is briefly introduced. This section is inspired by [8] which gives a useful introduction into optimal control theory for engineers and numerous references to related literature.
Whenever a dynamic system has a degree of freedom, some form of control is necessary. The general aim of a control system is to manipulate the behaviour of a dynamic system in an intended manner, for instance, to ensure stability against disturbances. The most challenging aim is optimal behaviour. Optimisation in terms of this paper means minimising a certain objective function $J$ over the time interval $t \in [t_0, t_e]$. $J$ is also called performance index, cost function, or optimality criterion. In context of optimal control, the Lagrange form

$$J = \int_{t_0}^{t_e} L\left(\boldsymbol{x}(t), \boldsymbol{u}(t), t\right) dt \tag{1}$$

is often used to describe accumulative costs such as the fuel consumption. The dynamic system is usually described by its differential equation

$$\dot{\boldsymbol{x}}(t) = \boldsymbol{f}\left(\boldsymbol{x}(t), \boldsymbol{u}(t), t\right), \boldsymbol{x}(t_0) = \boldsymbol{x}_0 \tag{2}$$

in which $\boldsymbol{x}$ is the vector of system states, $\boldsymbol{u}$ is the control vector which is composed of the decision variables, and $\boldsymbol{x}(t_0) = \boldsymbol{x}_0$ is the initial state. Note that vectors and vector functions are denoted in bold letters.
Depending on the problem, optimisation can be separated into two general types which will be explained by taking the example of a general control loop (see Figure 2).

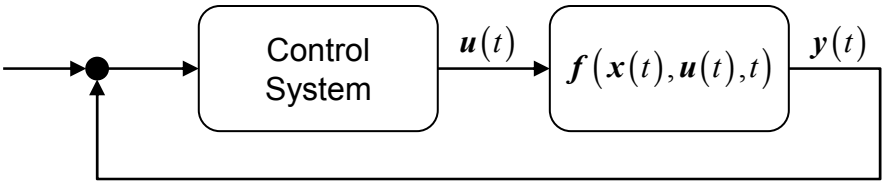


*Figure 2: General control loop including the dynamic system* $\boldsymbol{f}\left(\boldsymbol{x}(t), \boldsymbol{u}(t), t\right)$.

If the structure of the control system (e.g. a proportional control) is given, the remaining task will be to choose the optimal parameters (e.g. the gain). This classic discipline of control theory is called static optimisation. In contrast, dynamic optimisation deals with finding the optimal structure of the control system, i.e. the control input $\boldsymbol{u}(t)$. Optimal control of HEVs by means of energy management belongs to the latter. According to [12], the general scalar optimisation problem which is also called optimal control problem can be denoted by

$$\begin{cases} \text{minimise} & J = \int_{t_0}^{t_e} L\left(\boldsymbol{x}(t), \boldsymbol{u}(t), t\right) dt \\ \text{subject to:} & \dot{\boldsymbol{x}}(t) = \boldsymbol{f}\left(\boldsymbol{x}(t), \boldsymbol{u}(t), t\right) \\ & \boldsymbol{g}\left(\boldsymbol{x}(t_e), t_e\right) = \boldsymbol{0} \\ & \boldsymbol{h}\left(\boldsymbol{x}(t), \boldsymbol{u}(t), t\right) \le \boldsymbol{0}. \end{cases} \tag{3}$$

Constraints on the finale states are denoted by $\boldsymbol{g}$. Physical limitations, which are crucial for controlling technical systems in reality, are formulated as time-dependent constraints on states and controls by $\boldsymbol{h}$. The optimal control problem is solved over the horizon $t \in [t_0, t_e]$, which is given by a driving cycle.

## 2.1 Driving cycles and longitudinal vehicle dynamics

This paper uses real-world driving cycles which have been obtained from public transportation. The driving cycles are collected by measuring the velocity and other quantities of several hybrid buses during service on a single bus line. Its route topology is extracted from a map based on the measured GPS coordinates. As can be seen in Figure 3, the route has a length of approximately 38 km and is both flat and hilly with a maximum altitude difference of 187 m. In total, 151 cycles from about one year of driving are available which incorporate the influences of different drivers, amount of passengers, day times, seasons and various traffic disturbances. In average, the bus stops 93 times and travels at a speed of about 28 km/h on that specific bus line (see Figure 3).

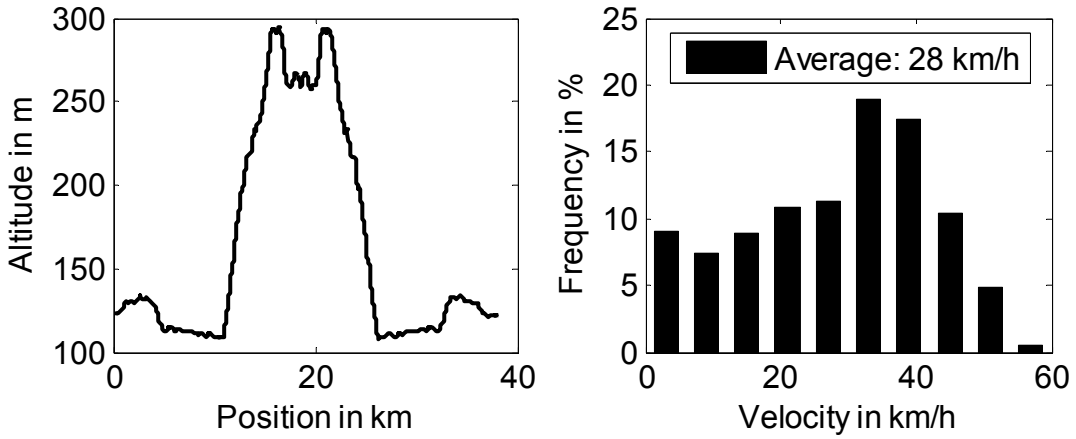


*Figure 3: Altitude profile of the investigated bus line (left) and exemplary velocity histogram of a common driving cycle (right). In total, 151 driving cycles on that bus line are used for simulations in this paper.*

The driving cycles have a constant sample time $\Delta t$ of a second which is directly adopted to the problem formulation later on. The discrete time samples of each cycle are indicated by

$$k = [0, ..., N_\mathrm{t} - 1],\ N_\mathrm{t} = \frac{t_\mathrm{e} - t_0}{\Delta t}, \tag{4}$$

in which $t_0$ and $t_\mathrm{e}$ is time at the beginning and at the end, respectively. In order to ideally follow a given driving cycle, which is denoted by a time-discrete velocity $v(k) \geq 0$ and a position-dependent road grade $\alpha(s)$ trajectory, the propulsion system has to deliver the wheel torque

$$T_\mathrm{W}(k) = \left(m \cdot a(k) + F_\alpha(\alpha(s)) + F_\mathrm{a}(a(k), v(k))\right) r \tag{5}$$

where

$$a(k) = \frac{v(k+1) - v(k)}{\Delta t} \tag{6}$$

is the acceleration,

$$s(k+1) = s(k) + \frac{v(k) + v(k+1)}{2} \Delta t \tag{7}$$

is the position on the route, $F_\alpha$ includes the rolling friction resistance and the grade resistance, $F_a$ denotes the aerodynamic drag force and $r$ is the dynamic rolling radius of the wheels. The total vehicle mass including rotational masses $m$ is assumed to be constant. This means that fluctuations in the number of passengers are neglected. For the sake of clarity, the dependency on discrete time $k$ is omitted hereafter whenever possible.

## 2.2 Series hybrid electric drivetrain

A simplified schematic of the propulsion system is depicted in Figure 4. The vehicle's prime mover is an engine-generator unit (EGU) which drains fuel energy $E_f$ from the fuel tank along a specific driving cycle. The electric energy storage (EES) with energy content $E_S$ can be charged by the EGU and by recuperating braking energy from the electric motor (EM). Furthermore, it can support the EGU in covering the electric power demand

$$P = \tilde{P}_M + P_A , \tag{8}$$

where $\tilde{P}_M$ is the electric power of the EM and $P_A$ is the electric power demand of the auxiliary loads, e.g. air condition and air compressor. The power balance of the electric intermediate circuit is denoted by

$$P_G + P_S - P = 0 , \tag{9}$$

in which $P_G$ and $P_S$ denotes the electrical EGU and EES output power, respectively.

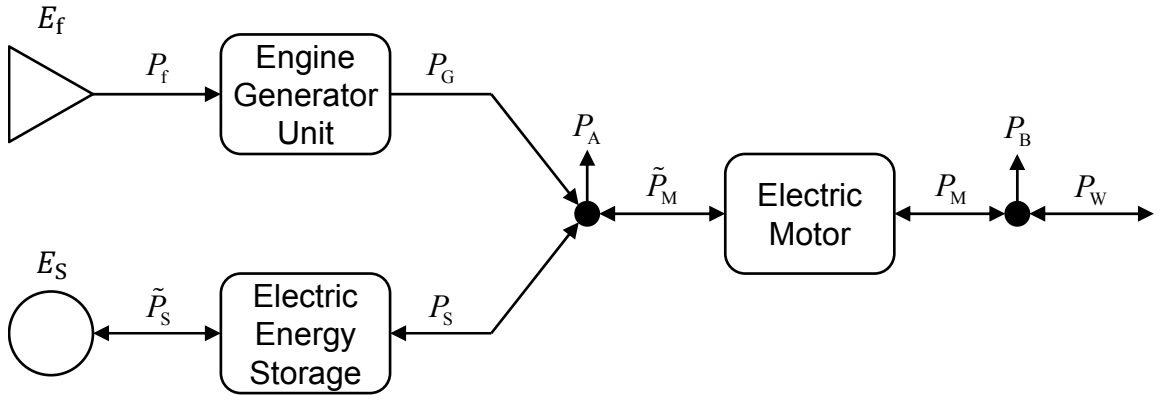


*Figure 4: Sketch of the drivetrain of the series hybrid electric city bus based on [12].*

The EM is connected to the driving axle through a constant transmission ratio $\gamma$. In addition to the required wheel torque, the dissipative losses of the transmission

$$T_{\mathrm{T,d}} = \begin{cases} \left(T_{\mathrm{W}}^2 \cdot c_{\mathrm{T},1} + T_{\mathrm{W}} \cdot c_{\mathrm{T},2} + c_{\mathrm{T},3}\right)\dfrac{1}{\gamma} & \text{if } v > 0 \\ 0 & \text{else} \end{cases} \tag{10}$$

have to be covered where $c_{\mathrm{T},1}$, $c_{\mathrm{T},2}$ and $c_{\mathrm{T},3}$ are constant values. The EM is designed to realise the utilised driving cycles. Nevertheless, the EM torque $T_{\mathrm{M}}$ and rotational speed

$$\omega_{\mathrm{M}} = \frac{v}{r}\gamma \tag{11}$$

are limited to the allowed bounds, i.e.

$$T_{\mathrm{M}} \in \left[T_{\mathrm{M,min}}, T_{\mathrm{M,max}}\right], \quad \omega_{\mathrm{M}} \in \left[\omega_{\mathrm{M,min}}, \omega_{\mathrm{M,max}}\right]. \tag{12}$$

Due to the facts that real driving cycles are used throughout this paper and $\gamma$ is constant, the speed boundaries are per se satisfied. During the braking process, however, the deliverable negative torque of the EM can be insufficient. In this case, the friction brakes are assumed to provide the additional braking torque $T_{\mathrm{B}} \geq 0$, i.e.

$$T_{\mathrm{M}} = \frac{T_{\mathrm{W}}}{\gamma} + T_{\mathrm{T,d}} - T_{\mathrm{B}}\,. \tag{13}$$

For a given mechanic power

$$P_{\mathrm{M}} = T_{\mathrm{M}} \cdot \omega_{\mathrm{M}} \tag{14}$$

the EM causes dissipative losses

$$P_{\mathrm{M,d}} = \begin{cases} P_{\mathrm{M}} \cdot \left(1 - \dfrac{1}{f_{\mathrm{M}}\left(T_{\mathrm{M}}, \omega_{\mathrm{M}}\right)}\right) & \text{if } T_{\mathrm{M}} \geq 0 \\ P_{\mathrm{M}} \cdot \left(f_{\mathrm{M}}\left(T_{\mathrm{M}}, \omega_{\mathrm{M}}\right) - 1\right) & \text{else} \end{cases}, \tag{15}$$

where $f_{\mathrm{M}}$ is the static efficiency map yielding

$$\tilde{P}_{\mathrm{M}} = P_{\mathrm{M}} + P_{\mathrm{M,d}}\,. \tag{16}$$

When the power demand (8) can be covered entirely by the electric storage, the EGU can be turned off at any time. Therefore, the EGU state is introduced by

$$\sigma \in \left\{\mathrm{off} = 0, \mathrm{on} = 1\right\}. \tag{17}$$

When the EGU is turned on, the generator accelerates the engine to a certain rotational speed causing $P_{\mathrm{G}} < 0$ while fuel is injected at the same time. This procedure lasts the time $t_{\mathrm{start}}$ and drains the energy $E_{\mathrm{f,start}}$ and $E_{\mathrm{G,start}}$ from the fuel tank and the EES, respectively. If the EGU is turned off, no fuel will be injected nor will electric energy be consumed or provided. The relating fuel power is denoted by

$$P_{\mathrm{f}} = \begin{cases} E_{\mathrm{f,start}} / \mathrm{t}_{\mathrm{start}} & \text{if } \sigma(k) = 0 \wedge \sigma(k+1) = 1 \\ f_{\mathrm{G}}(P_{\mathrm{G}}) & \text{if } \sigma(k) = 1 \wedge \sigma(k+1) = 1 \\ 0 & \text{else.} \end{cases} \tag{18}$$

The static map $f_{\mathrm{G}}$ expresses all dissipative losses occurring during the conversion from fuel energy to electric energy at the EGU's power output. In contrast to parallel hybrid electric vehicles, the engine speed is decoupled from the wheel speed. Thus, any output power can be provided with maximum achievable efficiency resulting in high efficiency over a wide operation range (see Figure 5). Note that the EGU still consumes fuel when idling ( $P_{\mathrm{G}} = 0$ ).

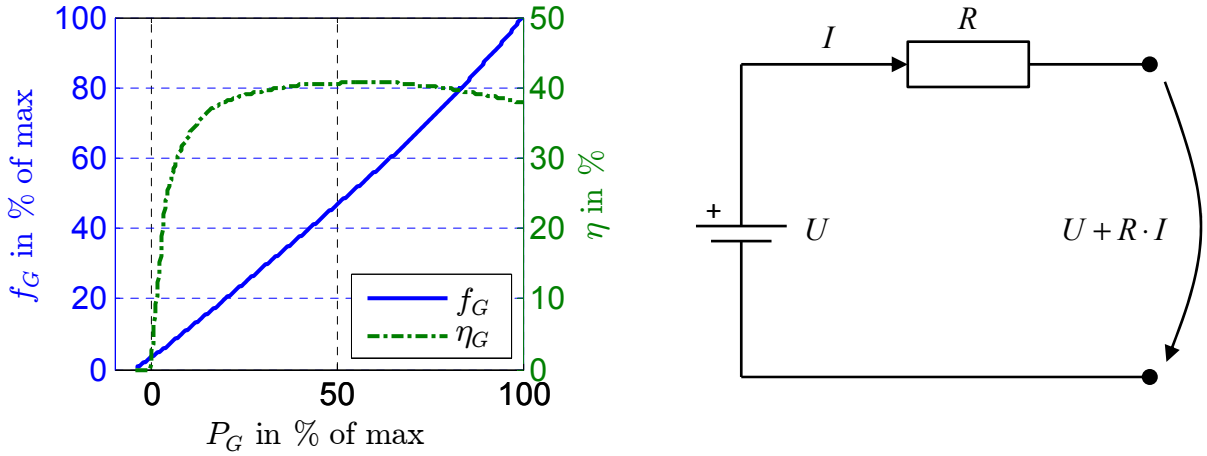


*Figure 5: Normalized static fuel and efficiency map of the engine-generator unit (left) and equivalent circuit model of the electric energy storage (right). The voltage source $U$ and the resistance $R$ are assumed to be constant.*

The EGU states impose constraints on the EGU's electric output power

$$P_{\mathrm{G}} = \begin{cases} -E_{\mathrm{G,start}} / \mathrm{t}_{\mathrm{start}} & \text{if } \sigma(k) = 0 \wedge \sigma(k+1) = 1 \\ \left[ P_{\mathrm{G,min}}, P_{\mathrm{G,max}} \right] & \text{if } \sigma(k) = 1 \wedge \sigma(k+1) = 1 \\ 0 & \text{else.} \end{cases} \tag{19}$$

This means that in the first case the EES has to cover the negative EGU power in addition to the power demand $P$ given by (8). In the second case, $P_{\mathrm{G}}$ can take any values between $P_{\mathrm{G,min}}$ and $P_{\mathrm{G,max}}$. Otherwise, the output power will equal zero.

The EES which is assumed to be of $LiFePo_4$ type is modelled as voltage source $U$ in series with a resistance $R$ (see Figure 5), which are both assumed to be constant. This assumption is important for the algorithm discussed later on. The chemical power is denoted by

$$\tilde{P}_{\mathrm{S}} = I \cdot U = P_{\mathrm{S}} + I^2 \cdot R \tag{20}$$

The current is a function of the output power $P_{\mathrm{S}}$ and can be obtained by rearranging (20) to

$$I(P_{\mathrm{S}}) = \frac{U - \sqrt{U^2 - 4R \cdot P_{\mathrm{S}}}}{2R}. \tag{21}$$

A positive current denotes depletion of the EES, which means a decrease of the charge $Q$. The system dynamics of the EES are denoted by

$$Q(k+1) = Q(k) - I\left(P_{\mathrm{S}}(k)\right) \cdot \Delta t \,. \tag{22}$$

Physical limitations of the EES impose constraints on the current

$$I \in \left[I_{\min}, I_{\max}\right] \tag{23}$$

and on the charge

$$Q \in \left[Q_{\min}, Q_{\max}\right]. \tag{24}$$

By introducing the state of charge (SOC)

$$\xi = \frac{Q}{Q_0} \tag{25}$$

where $Q_0$ is the nominal EES capacity, the charge can conveniently be denoted by a dimensionless quantity which will be used later in this paper.

### 2.3 Mixed-integer optimisation problem

The aforementioned series hybrid electric drivetrain has two freedoms, namely the power split (9) and EGU state $\sigma$ (17) which is controlled by the continuous decision variable $P_{\mathrm{S}}$ and the integer decision variable

$$u_\sigma \in \left\{\text{turn off} = -1,\ \text{stay} = 0,\ \text{turn on} = 1\right\}, \tag{26}$$

respectively. Accordingly, the mixed-integer control vector is represented by

$$\boldsymbol{u}(k) = \left(P_{\mathrm{S}}(k), u_\sigma(k)\right)^{\mathrm{T}} \tag{27}$$

where the continuous decision variable is constrained by transferring (19), i.e.

$$P_{\mathrm{S}}(k) = \begin{cases} P(k) + \beta_{\mathrm{G}} & \text{if } \sigma = 0 \wedge u_\sigma = 1 \\ \left[P'_{\mathrm{S,min}} \cdot \sigma(k), P'_{\mathrm{S,max}} \cdot \sigma(k)\right] & \text{if } \sigma = 1 \wedge u_\sigma = 0 \\ P(k) & \text{else.} \end{cases} \tag{28}$$

Therein, the additional electric energy demand for turning the EGU on is introduced as penalty $\beta_{\mathrm{G}} = E_{\mathrm{G,start}} / t_{\mathrm{start}}$ and the constraints on the operating range of $P_{\mathrm{G}}$ (19) and EES current $I$ (23) are merged substituting (23) in (20) to form a new EES minimum and maximum output power

$$\begin{aligned} P'_{\mathrm{S,min}} &= \max\left\{P_{\mathrm{S,min}}; \min\left\{P_{\mathrm{S,max}}; P(k) - P_{\mathrm{G,max}}\right\}\right\} \text{ and} \\ P'_{\mathrm{S,max}} &= \min\left\{P_{\mathrm{S,max}}; \max\left\{P_{\mathrm{S,min}}; P(k) - P_{\mathrm{G,min}}\right\}\right\}, \end{aligned} \tag{29}$$

respectively. Furthermore, the integer decision variable is constrained by

$$u_\sigma(k)=\begin{cases}[0,1] & \text{if } \sigma(k)=0\\ [-1,0] & \text{if } \sigma(k)=1.\end{cases} \tag{30}$$

The mixed-integer state vector is composed of the EES charge and the EGU state, i.e.

$$\boldsymbol{x}(k)=\left(Q(k),\sigma(k)\right)^{\mathrm{T}} \tag{31}$$

Regarding $\sigma$, it is assumed that the transition to on and off takes place within $\Delta t$. As a result and in accordance with (22), the mixed-integer system dynamics are denoted by

$$\boldsymbol{x}(k+1)-\boldsymbol{x}(k)=\boldsymbol{f}\left(\boldsymbol{x}(k),\boldsymbol{u}(k),k\right)=\begin{pmatrix}-I\left(P_{\mathrm{S}}(k)\right)\cdot\Delta t\\ u_\sigma(k)\end{pmatrix}. \tag{32}$$

The constraints on $\sigma$ (17) and $Q$ (24) are summarized by

$$\begin{pmatrix}\sigma\in\Sigma:=\{\text{off}=0,\ \text{on}=1\}\\ Q\in[Q_{\min},Q_{\max}]\end{pmatrix}. \tag{33}$$

The objective is to minimise the fuel consumption that is the accumulated fuel energy $E_{\mathrm{f}}$. Therefore, (18) is reformulated as a function of the state and decision variables at the current time

$$L\left(\sigma(k),P_{\mathrm{S}}(k),u_\sigma(k)\right)=\begin{cases}\beta_{\mathrm{f}} & \text{if } \sigma=0\wedge u_\sigma=1\\ f_{\mathrm{G}}\left(P_{\mathrm{S}}(k)-P(k)\right) & \text{if } \sigma=1\wedge u_\sigma=0\\ 0 & \text{else}\end{cases} \tag{34}$$

in which the additional fuel consumption for turning the EGU on is included as penalty $\beta_{\mathrm{f}}=E_{\mathrm{f,start}}/t_{\mathrm{start}}$.

The *optimal control problem* $\Pi$ is as follows. For a given driving cycle find the optimal control trajectory

$$\boldsymbol{\pi}^*=\left(\boldsymbol{u}^*(0),\boldsymbol{u}^*(1),\ldots,\boldsymbol{u}^*(N_t-1)\right),\ \text{where}\ \boldsymbol{u}^*(k)=\left(P_{\mathrm{G}}^*(k),u_{\sigma}^*(k)\right)^{\mathrm{T}} \tag{35}$$

which minimises the objective function

$$J=E_f=\sum_{k=0}^{N_t-1}L\left(\sigma(k),P_{\mathrm{S}}(k),u_\sigma(k)\right)\cdot\Delta t \tag{36}$$

and yields the optimal state vector $\boldsymbol{x}^*(k)=\left(Q^*(k),\sigma^*(k)\right)^{\mathrm{T}}$ at each time $k$. The optimal solution, which is marked by *, is subject to (26)-(33) and to the conditions on the initial and final states

$$\boldsymbol{x}(N_t)=\boldsymbol{x}(0)=\begin{pmatrix}\frac{Q_{\min}+Q_{\max}}{2}\\ 0\end{pmatrix}. \tag{37}$$

By imposing (37) on $\Pi$ the EES energy content at the end is kept the same as at the beginning of the horizon, which means charge sustaining. Note that $Q$ is equivalent

to the EES energy content because the voltage is assumed to be constant. Furthermore, the driving cycle starts and ends with disengaged EGU. Incorporating these boundary conditions ensures comparability of the results among different driving cycles or control trajectories $\boldsymbol{\pi}$. In the following sections, two different approaches to determine the optimal control trajectory $\boldsymbol{\pi}^*$ are introduced.

# 3 Optimal control using deterministic dynamic programming

Dynamic programming is based on Bellman's principle of optimality. It states that for a given optimal control trajectory $\boldsymbol{\pi}^*$, the truncated policy $\left(\boldsymbol{u}^*(k), \boldsymbol{u}^*(k+1), \ldots, \boldsymbol{u}^*(N_t-1)\right)$ is also optimal for a sub-problem starting at time $k,\ 0<k<N_t$ [8]. For a more intuitive explanation, suppose an auto travel analogy: if the fastest route from Dresden to Wiesloch passes Nurnberg, then the Nurnberg to Wiesloch portion of this route is also the fastest route for a trip starting in Nurnberg and ending in Wiesloch. The principle of optimality is incorporated by breaking the whole decision problem down into sub-problems which is described through the Bellman equation

$$J_k^*\left(\boldsymbol{x}(k)\right) = \min_{\boldsymbol{u}(k)}\left[ L\left(\boldsymbol{x}(k), \boldsymbol{u}(k)\right)\cdot \Delta t + J_{k+1}^*\left(\boldsymbol{x}(k+1)\right)\right], k = N_t-1, \ldots, 1, 0 \tag{38}$$

at each time $k$ [3]. This procedure is called DP algorithm and $J_k^*\left(\boldsymbol{x}(k)\right)$ is the so-called optimal cost-to-go at state $\boldsymbol{x}(k)$ and time $k$ [3]. The DP algorithm commonly begins at $k = N_t - 1$ with $J_{N_t}^*\left(\boldsymbol{x}(N_t)\right) = 0$, but it is also possible to start from $k=1$ which yields the optimal cost-to-arrive. The optimal control vector at each step is given by the argument minimising the right-hand side of (38). This procedure is repeated for each $k$ to obtain the optimal control trajectory $\boldsymbol{\pi}^*$.
Depending on the optimisation problem, (38) can be solved analytically yielding a control law. However, in many practical cases this is not possible and numerical execution of the Bellman equation is necessary [3]. Since computational implementation of DP usually requires discretised state and control space [20], it is also well suited for solving mixed-integer optimisation problems. A comprehensive introduction into dynamic programming and its application to discrete-time dynamic systems can be found in the commonly cited text book [3]. Hereinafter, only the basic concept of DP is introduced since a detailed explanation of the numerical algorithm is beyond the scope of this paper.

## 3.1 Numerical implementation of the DP algorithm

The DP algorithm (38) is applied to the optimal control problem $\Pi$ as has been described in the preceding section. However, analytical solution is not possible since the instantaneous costs $L$ (36) are determined using maps for several components. Therefore, numerical execution of the DP algorithm is necessary which means minimisation of (38) for each value of $\boldsymbol{x}(k)$ [3]. Therefore, discretisation of the state variables is necessary. Since the EGU state $\sigma$ is of integer type, only the EES charge $Q$

is discretised using a grid of the size of $N_Q$ samples. The grid size determines the smallest possible change in the EES charge

$$\Delta Q = \frac{Q_{\max} - Q_{\min}}{N_Q} \tag{39}$$

within a time step $\Delta t$. Furthermore, the control vector is often discretised as well (27) [20]. In doing so, the instantaneous costs $L\left(\sigma(k), P_S(k), u_\sigma(k)\right) \cdot \Delta t$ and (32) can be solved directly, which yields the next state $\boldsymbol{x}(k+1)$. However, since $\boldsymbol{x}(k+1)$ can only attain values on the grid, interpolation is required. This issue is avoided by determining the control vector through inversion of the state dynamics (32) using nested loops over all reachable states $\boldsymbol{x}(k+1)$ starting from each value of $\boldsymbol{x}(k)$ as described in [31]. Thus, the discrete step size of the decision variable $\Delta P_S$ is determined by $\Delta Q$ according to (20) and (22). As a consequence, $\Delta Q$ has to be sufficiently small, so that $\Delta P_S$ allows for maximum EGU efficiency, which is also true in case of a discretized control vector.

In order to actually calculate $J_k^*\left(x(k)\right)$, the numerical algorithm has to differentiate between the three cases introduced in (34), namely the EGU is engaged, turned on and turned off or not engaged. Therefore, the algorithm is implemented using five nested loops, one over the time $k$ and two loops over each value of state variables ($Q$ and $\sigma$) at time $k$ and $k+1$. For the corresponding flow-chart, the reader is referred to [31] where the basic scheme is described. For the second and third case, $\boldsymbol{x}(k+1)$ can directly be calculated using the model equations without loops because the EES has to cover the whole power demand according to (9), anyway. This means that when starting from a specific value $Q(k)$ the value of $Q(k+1)$ is prescribed since $P_S = P$. Due to discretisation, $Q(k+1)$ is rounded down to the next discrete value implying $P_S \geq P$. For example, if $P > 0$, rounding down of $Q(k+1)$ will cause an artificial greater depletion of the EES since the power demand must not be undercut. However, if $P < 0$, some amount of the regenerated energy (due to braking) will not be stored in the EES. Hence, $N_Q$ significantly affects the accuracy of the DP.

### 3.2 Sensitivity analysis of the charge discretisation

A sparse discretisation of $Q$ yields to low solution accuracy due to rounding down $Q(k+1)$ which results in an energy difference. The accumulative sum of this energy difference is called discretization error. Consequently, the discretization error decreases with growing $N_Q$. Unfortunately, $N_Q$ exponentially affects computational effort and memory consumption [8]. Thus, the maximum accuracy is limited by means of both available memory and time for computation. Therefore, a sensitivity analysis of the grid size for a particular driving cycle shall reveal reasonable values for $N_Q$. The results are depicted in Figure 6, in which $J^*$ is the optimal cost-to-go starting

from the initial state (i.e. the fuel consumption), $t_{\mathrm{DP}}$ is the expended computation time, $t_{\sigma=1}$ is the accumulated time that $\sigma = 1$ and $\delta_{DP}$ is the discretisation error.

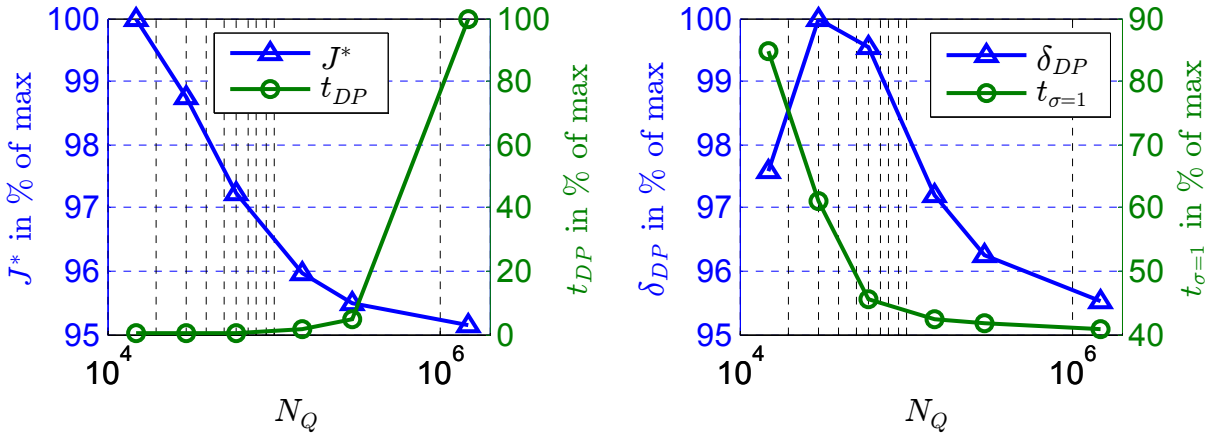


*Figure 6: Normalized fuel consumption $J^*$ and expended computation time $t_{\mathrm{DP}}$ (left), normalized accumulated EGU-on time $t_{\sigma=1}$ and discretization error $\delta_{DP}$ (right). High accuracy in terms of minimal fuel consumption is only achieved with fine discretization. The expended computation time for the finest discretization is about 56 hours.*

The optimal cost-to-go $J^*$ approaches its lower limit at the largest value of $N_Q$. At the same time, the expended computation time $t_{\mathrm{DP}}$ exponentially increases due to the curse of dimensionality. As anticipated, the discretisation error $\delta_{DP}$ approaches its minimum at the largest values of $N_Q$. However, the maximum error does not occur at minimum grid size. This can be explained by changes of $t_{\sigma=1}$. With decreasing $N_Q$, DP tends to keep the EGU engaged for longer periods of time because quantization errors only occur during pure electric driving ($\sigma = 1$). For the smallest grid size, DP keeps the EGU engaged for about 85% of the whole driving cycle which substantially reduces the quantization error. Nevertheless, $J^*$ steadily increases since large values of $t_{\sigma=1}$ imply that the EGU is operated in points of lower efficiency for a longer period of time.

Although the maximum grid size used in this study is not yet limited by available memory, the maximum computation time $t_{\mathrm{DP}}$ in Figure 6 is about 56 hours. However, even with medium grid size, solving $\Pi$ for a single driving cycle would still last several minutes. Since this paper pursues the objective to study the trade-off between fuel consumption and driveability, the optimal control problem has to be solved thousands of times due to parameter variation and several driving cycles. Hence, a faster approach is needed.

# 4. Introduction of the PMP-DP method

In addition to DP, a second method for solving optimal control problems was introduced by the mathematician L. S. Pontryagin [8]. In contrast to the classical calculus of variations, Pontryagin's maximum principle (PMP) incorporates constraints on the control vector. A comprehensive introduction to PMP and criteria for optimality as well as further references can be found in [3] and [8]. This section gives a brief introduction of the basic equations and necessary conditions for optimality for $\Pi$. A fundamental equation of PMP is the Hamiltonian function

$$H\left(\boldsymbol{x}(k),\boldsymbol{u}(k),\boldsymbol{\psi}(k),k\right)=L\left(\boldsymbol{x}(k),\boldsymbol{u}(k),k\right)-\boldsymbol{\psi}^{T}\cdot\left(\boldsymbol{f}\left(\boldsymbol{x}(k),\boldsymbol{u}(k),k\right)\right), \tag{40}$$

in which $\boldsymbol{\psi}^{T}$ denotes the vector of costate variables which adjoin the system dynamics to the objective function. The optimal control problem can be solved through differentiation of the Hamiltonian with respect to the control vector which is

$$\frac{\partial H}{\partial \boldsymbol{u}}=\boldsymbol{0}\,. \tag{41}$$

However, this necessary condition is only valid for unconstrained $\boldsymbol{u}$. In fact, technical systems do pose constraints on the control vector, wherefore (41) can no longer be used [8]. Instead, the maximum principle replaces (41) with the demand that $H$ shall be maximised or minimised by optimal choice of $\boldsymbol{u}$ which denotes the necessary condition for optimality. Instead of directly minimising the objective function as DP does, the task is now to minimise the Hamiltonian. The optimal state and control trajectories must satisfy the system dynamics (32), the conditions on the initial and final states (33), and the costate dynamics [14]

$$\boldsymbol{\psi}^{*}\left(k+1\right)-\boldsymbol{\psi}^{*}\left(k\right)=-\frac{\partial H}{\partial \boldsymbol{x}} \tag{42}$$

as well as

$$H\left(\boldsymbol{x}^{*}(k),\boldsymbol{u}^{*}(k),\boldsymbol{\psi}^{*}(k),k\right)\leq H\left(\boldsymbol{x}^{*}(k),\boldsymbol{u}(k),\boldsymbol{\psi}^{*}(k),k\right) \tag{43}$$

for each time $k$ with respect to the control constraints (28). As a consequence of the numerous differentiations, PMP cannot be applied to mixed-integer problems and is thus restricted to problems with continuous states. Hence, a combination of DP and PMP is used, which is an extension of the approach proposed in [20]. The so-called PMP-DP method utilises DP to calculate engine state while PMP determines the power split subject to the aforementioned optimality conditions.

## 4.1 Application of the maximum principle

The maximum principle is applied for determining the power split, which means to find the EES output power $P_{\mathrm{S}}(k)$ at each time $k$ for a given driving cycle. This scalar sub-problem only considers the EES related system state $Q$. Substitution of both (34) and the first element of (32) in (40) yields the Hamiltonian function of the sub-problem

$$H\left(\sigma(k),P_{\mathrm{S}}(k),u_{\sigma}(k),\psi(k)\right)=L\left(\sigma(k),P_{\mathrm{S}}(k),u_{\sigma}(k)\right)-\psi(k)\cdot I\left(P_{\mathrm{S}}(k)\right). \tag{44}$$

Note that $\sigma(k)$ and $u_{\sigma}(k)$ are given by DP. For ease of notation, the dependencies of $H$ are omitted hereafter, which is expressed by $(.)$. By introducing the equivalence factor as

$$\lambda=-\frac{\psi}{U} \tag{45}$$

and substituting of the EES current $I$ with the chemical power $\tilde{P}_{\mathrm{S}}$ according to (20), the Hamiltonian function becomes

$$H(.)=L\left(\sigma(k),P_{\mathrm{S}}(k),u_{\sigma}(k)\right)+\lambda(k)\cdot\tilde{P}_{\mathrm{S}}\left(P_{\mathrm{S}}(k)\right). \tag{46}$$

Due to the case differentiation in (34) and constraints on $P_{\mathrm{S}}$ (28), the Hamiltonian of the sub-problem is finally denoted by

$$H(.)=\begin{cases}\beta_{\mathrm{f}} & +\lambda(k)\cdot\tilde{P}_{\mathrm{S}}\left(P+\beta_{\mathrm{G}}\right) & \text{if } \sigma=0\wedge u_{\sigma}=1\\ f_{\mathrm{f}}\left(P_{\mathrm{S}}(k)-P(k)\right) & +\lambda(k)\cdot\tilde{P}_{\mathrm{S}}\left(P_{\mathrm{S}}\right) & \text{if } \sigma=1\wedge u_{\sigma}=0\\ 0 & +\lambda(k)\cdot\tilde{P}_{\mathrm{S}}(P) & \text{else,}\end{cases} \tag{47}$$

in which $P_{\mathrm{G}}$ is substituted with $P_{\mathrm{S}}-P$ according to (9). Given $\lambda(k)$, $P_{\mathrm{S}}(k)$ is calculated through minimisation of (47) at each time $k$ for any trajectory of $\sigma(k)$ and $u_{\sigma}(k)$. In this paper, this is done numerically discretising $P_{\mathrm{S}}$ within its boundaries (29) except when $P_{\mathrm{S}}$ is prescribed due to constraints (28).

Since (47) is not a function of the state variable, plugging (45) in (42) yield a constant equivalence factor, i.e.

$$\lambda(k+1)-\lambda(k)=\frac{\partial H\left(\sigma(k),P_{\mathrm{S}}(k),u_{\sigma}(k),\lambda(k)\right)}{\partial Q}=0. \tag{48}$$

As a result of this, $\lambda^{*}(k)=\lambda^{*}(0)=\lambda_{\mathrm{opt}}$. Thus, a root finding algorithm can be applied in order to obtain the constant optimal equivalence factor $\lambda_{\mathrm{opt}}$ [1], [14]. In [16], a benchmark of several algorithms shows that the bisection algorithm provides good trade-off between robustness, complexity and accuracy. Hence, the bisection algorithm is used in the present paper. Since the root finding is done numerically in an iterative manner, the final state condition (37) has to be relaxed to

$$\left|Q(N)-Q(0)\right|<q \tag{49}$$

with a predefined small number $q\geq 0$ [20]. The bisection method is terminated if (49) is satisfied or if the number of iterations exceeds a certain threshold. The latter is due to characteristics of the Hamiltonian function which are explained in the following.

Therefore, Figure 7 shows the Hamiltonian function (47) and its derivative $H'(.)$ at certain $\lambda$ and $P$ provided that $P_{\mathrm{S}}$ is not predefined by constraints, i.e. for $\sigma=1\wedge u_{\sigma}=0$. Note that both functions are plotted against the EGU output power $P_{\mathrm{G}}$ instead of $P_{\mathrm{S}}$ because this allows for a more convenient depiction. Due to the chosen

values of $\lambda$ and $P$, the minimum of $H(.)$ occurs at about $P_{\mathrm{G}} = 0.55 \cdot P_{\mathrm{G,max}}$ which is the root of $H'(.)$. The value of $P_{\mathrm{S}}$ is immediately determined by (9). Variation of $\lambda$ and $P$ offsets $H'(.)$ vertically and shifts the root, accordingly. Since $H'(.)$ is not monotonically increasing due to the map $f_{\mathrm{G}}$, distinct jumps between the roots will occur which lead to discontinuities in the decision variable (see Figure 12). Moreover, the different cases of (47) induce discontinuities in the Hamiltonian function similar to [20]. Likewise, satisfaction of (49) cannot be guaranteed for all termination criteria. Nevertheless, the author of [20] showed that PMP is still applicable in determining the power split if the constant equivalence factor is chosen properly.

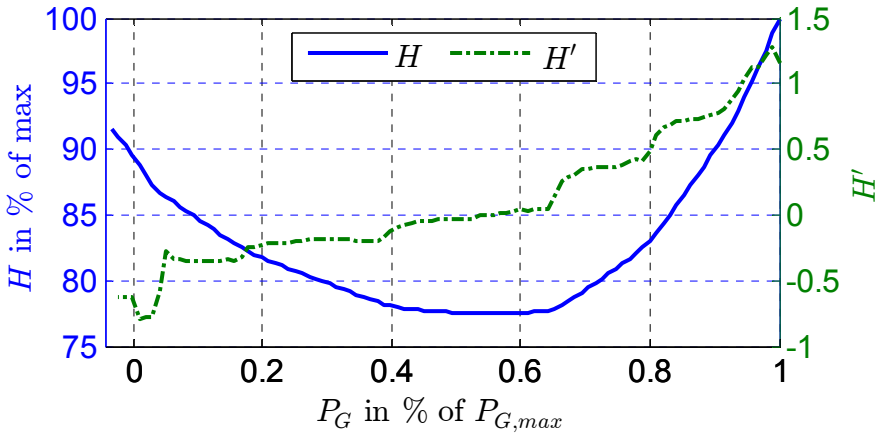


*Figure 7: Normalized Hamilton function and its derivative at certain $\lambda$ and $P$. Due to the erratic roots of the Hamilton function, the resulting control will possess discontinuities which is shown later on.*

A fundamental assumption of [20] is that the charge boundaries are never exceeded which simplifies the control problem because no effort has to be spent in order to ensure the state constraints. However, this assumption might not be valid in reality because of multiple disturbances and uncertainties. PMP can be extended to incorporate constraints on the states, which is, however, complicated [8]. Fortunately, this obstacle can be overcome by the following *separation algorithm* as proposed in [14] and [16]. First, the unconstrained two-point boundary problem is solved over the whole horizon, so that (49) is satisfied. Second, the time $k$ when the state boundary is exceeded the most is searched. Third, the initial trajectory is split in two sub-trajectories solving each as an unconstrained two-point boundary problem. Fourth, this procedure is repeated until none of the sub-trajectories exceed the state boundaries any more. A sketch of this principle can be seen in [31].

## 4.2 Combination of PMP and DP

As has been stated previously, PMP determines the power split along a given driving cycle with any trajectory $\sigma(k)$ and $u_{\sigma}(k)$. Thus, DP is applied with the aim of determining $u_{\sigma}^{*}(k)$ at each $k$, which yields $\sigma^{*}(k+1)$ according to (32). Therefore, a new objective function is introduced

$$J_{\mathrm{eq}} = \sum_{k=0}^{N_{\mathrm{t}}-1} C_{\mathrm{eq}}(k) \cdot \Delta t \tag{50}$$

in which

$$C_{\mathrm{eq}}(k) = H\left(\sigma(k), P_{\mathrm{S}}(k), u_{\sigma}(k), \lambda\right), \tag{51}$$

are the equivalent costs for a given $\lambda$, as proposed in [20]. The DP algorithm is implemented in the same manner as previously presented but now calculating the optimal equivalent cost-to-go

$$J_{\mathrm{eq},k}\left(\sigma(k)\right) = \min_{u_{\sigma}(k)}\left[C_{\mathrm{eq}}(k) \cdot \Delta t + J_{\mathrm{eq},k+1}\left(\sigma(k+1)\right)\right]. \tag{52}$$

Figure 8 shows a sketch of the entire PMP-DP algorithm, which will be explained in the following.

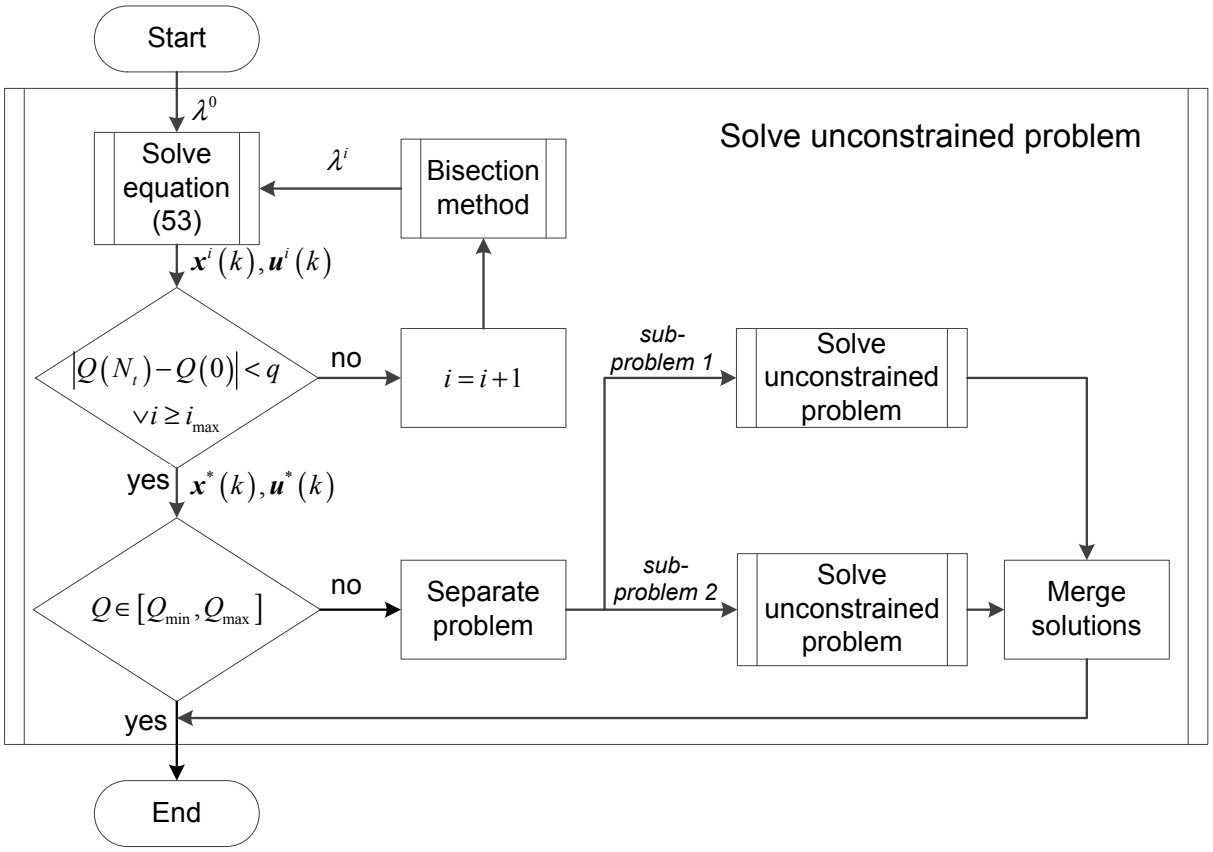


*Figure 8: Simplified flow chart of the PMP-DP method. The optimal control problem is solved in a recursive manner to ensure the constraints on the EES charge.*

At first, the iteration counter and the corresponding equivalence factor $\lambda^0$ is initialized by $i = 0$ and a constant value, respectively. Next, the function "solve unconstrained problem" is called, wherein (52) is solved as described in the previous paragraph yielding the state and control vector $\boldsymbol{x}^i(k)$ and $\boldsymbol{u}^i(k)$, respectively, at each time $k$. If the final condition (49) is not satisfied, the counter will be incremented and a new equivalence factor $\lambda^i$ will be determined using the bisection method. This procedure is repeated until the final condition (49) is satisfied or the maximum number of iterations $i_{\max}$ is reached. Afterwards, the state constraints (33) are checked. If the charge boundaries are exceeded, the control problem will be separated into two sub-

problems at the point where the absolute exceedance has its maximum. Both sub-problems are solved recursively calling the function “solve unconstrained problem” until all sub-problems satisfy the charge constraints. Note that DP satisfies the constraints on $\sigma$ per se.

However, solving (52) only yields the optimal control and state vector $\boldsymbol{u}^*(k)$ and $\boldsymbol{x}^*(k)$, respectively, if $\lambda_{\text{opt}}$ is determined correctly. Unfortunately, the authors of [14] only proved that the separation algorithm (including the bisection method), which determines the equivalence factor, is optimal for convex problems. Since $\Pi$ is non-convex, the results obtained by the PMP-DP method have to be validated.

### 4.3 Comparison to DP solution

For validation of the PMP-DP method, a comparison to the DP solution for the same driving cycle which was used in the discretisation sensitivity analysis is conducted. Therefore, the second finest grid size (see Figure 6) is used for calculating the DP solution since it offers a reasonable trade-off between accuracy and computation time. Figure 9 depicts the trajectories of the discretization error and the SOC.

In the DP solution, the discretization error is compensated through increased charging of the EES by the EGU, which results in additional fuel consumption. Furthermore, DP keeps SOC higher than PMP-DP in the middle of the driving cycle. Since PMP has been applied without discretisation of the charge, the PMP-DP method does not cause a discretisation error. Thus, PMP-DP achieves 0.4% lower fuel consumption which is merely due to the modest grid size of DP. Nevertheless, these results indicate that the PMP-DP solution is close to optimal which means that $\lambda_{\text{opt}}$ can actually be determined. Since only few seconds are expended to compute the solution on the same machine which was used for the discretisation sensitivity analysis, the PMP-DP method is utilised for investigating the trade-off between fuel economy and drivetrain activity later on.

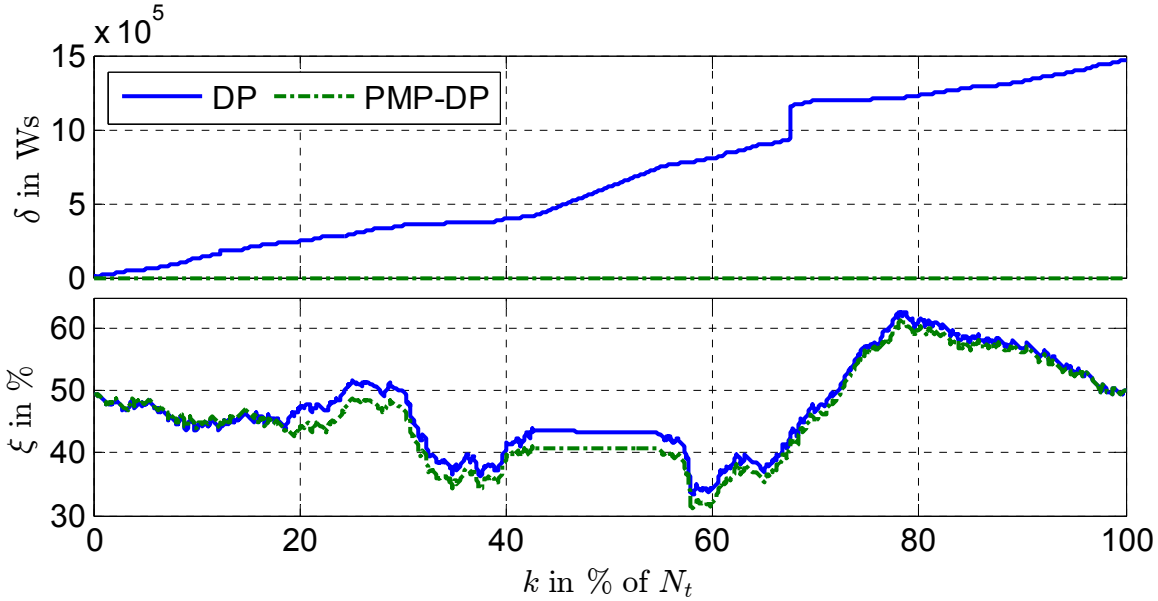


*Figure 9: Trajectories of the discretisation error $\delta$ (top) and state of charge $\xi$ (bottom) of the DP and PMP-DP solution. The differences between both SOC trajectories are due to the discretization error of the DP solution.*

### 4.4 Correction of fuel consumption

Since the final state conditions are relaxed by (49), deviations from the final charge setpoint $Q(N_t) = Q(0)$ can occur which are equally expressible by means of a SOC difference

$$\Delta\xi = \xi(N_t) - \xi(0). \tag{53}$$

Figure 10 shows $\Delta\xi$ for $q/Q_0 = 1\%$ among all driving cycles. Although the absolute average value of $\Delta\xi$ is smaller than $q/Q_0$, greater differences than 1% can occur which are due to the discontinuity in the Hamiltonian function and the position of its roots.

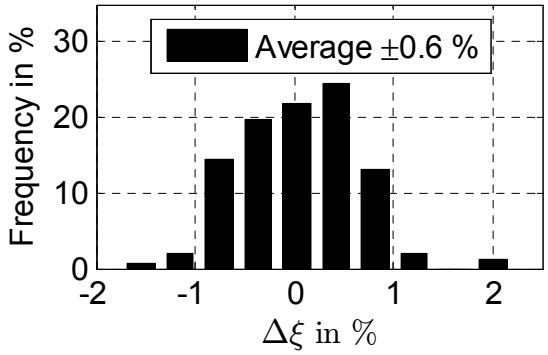


*Figure 10: State of charge difference $\Delta\xi$ from the setpoint for $q/Q_0 = 0.01$ among all driving cycles. Due to the discontinuity in the Hamiltonian function and the position of its roots, $\Delta\xi$ can be greater than the desired tolerance which means different final EES energy contents. Therefore, subsequent correction of fuel consumption is necessary.*

Any deviation from $\Delta\xi = 0$ causes a different final EES energy content which affects the fuel consumption. For example, if $\Delta\xi > 0$, the EES has been charged beyond setpoint and, therefore, additional fuel has been consumed. However, if $\Delta\xi < 0$, some part of the energy demand has been covered by the EES yielding decreased fuel consumption. In order to ensure comparability among different driving cycles, the fuel consumption has to be corrected in dependency of $\Delta\xi$.

However, there are few references in literature that specifically address this topic. Mostly, this fact is treated very briefly or is not mentioned at all. The following two publications consider a hybrid HEV on the New European Driving Cycle. While optimising a rule-based EMS, [6] observes a linear relationship between fuel consumption and final SOC, which is used to transform $\Delta\xi$ into equivalent fuel consumption. Also [27] states linear relationship between fuel consumption and final SOC by using various constant values of the decision variable. In contrast to [6], the linear relationship is divided into two branches due to the different efficiencies while charging and depleting the EES. The slope of either of these branches is used to convert $\Delta\xi$ into equivalent fuel consumption. Another related approach using ECMS can be found in [15], where the author proposes a fuel correction based on a constant worst-case equivalence factor. Moreover, if a certain threshold is exceeded, additional quadratic penalties will be introduced. However, the fuel consumption is only corrected for $\Delta\xi < 0$ but not for $\Delta\xi > 0$. This is motivated by two facts. Firstly, since the driving cy-

cle is not perfectly known in advance, the equivalence factor is not constant which will possibly cause non-linear relationship between fuel consumption and $\Delta\xi$. Secondly and consequently, the additional amount of energy stored in the EES does not necessarily lead to reduced fuel consumption in the (unknown) future.
However, none of the aforementioned authors applied knowledge of the optimal solution for correcting the fuel consumption. The approach presented in this paper takes advantage from knowing $\lambda_{\mathrm{opt}}$. Therefore, $\Delta\xi$ is transformed into equivalent fuel consumption which is added to the objective function (36) yielding the corrected fuel consumption

$$J^* = \lambda_{\mathrm{opt}} \cdot \Delta\xi \cdot Q_0 \cdot U + \sum_{k=0}^{N_\mathrm{t}-1} P_\mathrm{f}\left(\sigma(k), P_\mathrm{S}(k), u_\sigma(k)\right) \cdot \Delta t \,. \tag{54}$$

For validation of this approach, the uncorrected fuel consumption is calculated for a discrete set of feasible SOC setpoints $\xi_{\mathrm{set}}$ and a certain driving cycle. Starting from each of the resulting SOC values $\xi(N_t)$, which slightly differ from the setpoints, the corrected fuel consumption is calculated for $\xi_{\mathrm{set}}$. The difference between both can be regarded as artificially induced $\Delta\xi$ which is used for investigating the relative error of the costate-based fuel consumption. The relative error is the corrected fuel consumption divided by the actual fuel consumption at each discrete SOC value minus one. Figure 11 illustrates that the maximum relative error is about 0.2% and occurs only for large $\Delta\xi$ when the setpoint of $\xi(N_t)$ is near the lower boundary. Despite that, the relative error is negligible over a wide range of the SOC which means that the costate-based fuel correction is also valid for absolute values of $\Delta\xi$ greater than 2%.
Since all subsequent investigations are done using the PMP-DP method, all results with regard to fuel consumption will be based on (54). However, this will not be mentioned explicitly for the sake of convenience.

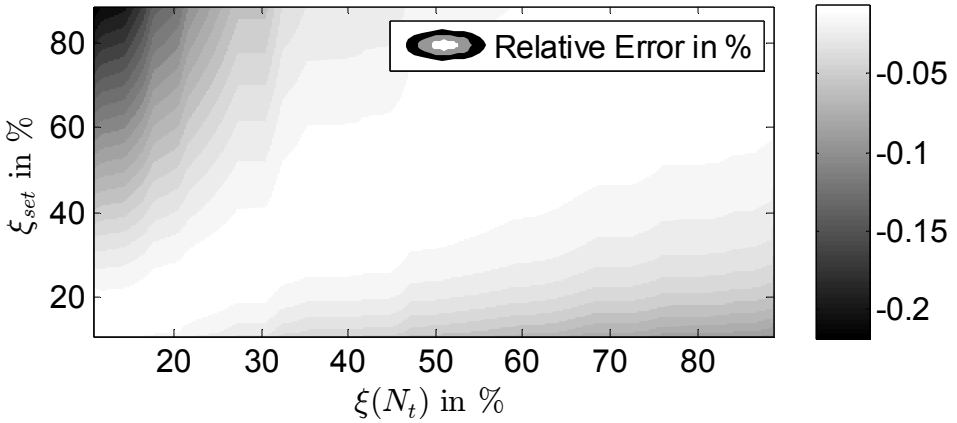


*Figure 11: Relative error of costate-based fuel correction. The plot has to be read as follows: the abscissa and the ordinate represent several final SOC $\xi(N_t)$ and several corresponding SOC setpoints $\xi_{\mathrm{set}}$. For example, if the final SOC is 20% and the setpoint is actually 80%, the relative error of the fuel correction will be about 0.1%.*

# 5. Trade-off between fuel consumption and drivetrain activity

In this section, the PMP-DP method is utilised in order to investigate the trade-off between fuel consumption and drivetrain activity based on simulations of numerous real-world driving cycles. At first, the term drivetrain activity is specified and corresponding measures are introduced.

## 5.1 Definition of measures for drivetrain activity

For $\Pi$, the drivetrain activity is constituted of changes in EGU operating point and state, both affected by the control vector $\boldsymbol{u}$. For example, changing $P_{\mathrm{G}}$ alters the operating point of the EGU (i.e. speed and torque), which can be distinguished by the passengers due to the engine noise. Thus, frequent toggling between distinct operating points should be avoided. Fortunately, if power demand $P$ and equivalence factor $\lambda$ are constant, optimal control will result in a constant power split. However, when $P$ toggles between particular values, driveability can be poor in terms of engine noise due to the discontinuities in the power split (see Figure 12).

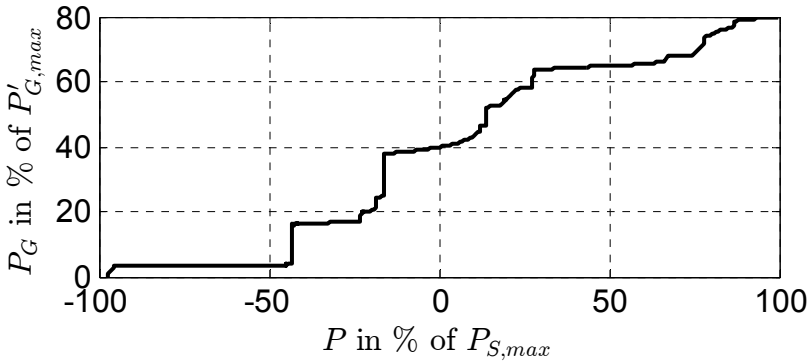


*Figure 12: Normalized EGU output power for $\sigma = 1$ over admissible $P$. The discontinuities, which are due to the run of the derivative of the Hamiltonian function $H'(.)$, can result in bad driveability in terms of engine noise.*

On the one hand, this issue strongly depends on driver and driving conditions. On the other hand, the discontinuities shown in Figure 12 can be avoided by approximating $f_{\mathrm{G}}$ (see Figure 5) with a polynomial, for instance. Therefore, this will not be subject of the driveability study of this work. Hence, merely changes of the EGU state are considered in terms of drivetrain activity in this paper. The indicator function

$$f_\sigma = \begin{cases} 1 & \text{if } \sigma(k-1) \neq \sigma(k) \\ 0 & \text{else} \end{cases} \tag{55}$$

shows when EGU events are produced. To quantify the drivetrain activity induced by the EMS for a particular driving cycle, the total number of EGU start and stop events

$$n_\sigma = \sum_{k=2}^{N_t} f_\sigma(k-1,k) \tag{56}$$

is used as metric, similar to [22]. Since this paper only investigates one specific bus line, there is no need to normalise $n_\sigma$. Another important aspect in terms of drivetrain

activity is the time span between two EGU events. Therefore, the vectors $\boldsymbol{t}_{on}$ and $\boldsymbol{t}_{off}$ are introduced which contain the time span of all periods where $\sigma = 0$ and $\sigma = 1$, respectively. For convenient notation, the symbol $t_\sigma$ is used when referring to either $\boldsymbol{t}_{on}$ and $\boldsymbol{t}_{off}$.

## 5.2 Impact of penalty costs for EGU starts

To account for the additional energy consumption for starting the EGU, the penalty costs $\beta_\mathrm{f}$ and $\beta_\mathrm{G}$ have been introduced in the objective function (36) and in the system dynamics (32), respectively. In the following, the impact of neglecting $\beta_\mathrm{f}$ and $\beta_\mathrm{G}$ on optimal control and fuel consumption is investigated. Therefore, $\Pi$ is reformulated and renamed as follows:

- $\Pi_1$ neglects the start costs, i.e. $\beta_\mathrm{f} = \beta_\mathrm{G} = 0$, and
- $\Pi_2$ incorporates the start costs, i.e. $\beta_\mathrm{f} = E_\mathrm{f,start} / t_\mathrm{start}$ and $\beta_\mathrm{G} = E_\mathrm{G,start} / t_\mathrm{start}$.

Note that $\Pi_2$ is introduced as a new symbol for the sake of convenient notation in the subsequent plots although it is equal to $\Pi$. In order to show the impact of neglecting the start costs in $\Pi_1$, $Q^*(k)$ and $J^*(k)$ are recalculated using a vehicle model that incorporates $\beta_\mathrm{f} = E_\mathrm{f,start} / t_\mathrm{start}$ and $\beta_\mathrm{G} = E_\mathrm{G,start} / t_\mathrm{start}$.

First, $\Pi_1$ and $\Pi_2$ are solved using PMP-DP for one driving cycle to investigate the effects on optimal control in detail (see Figure 13). Please keep in mind that each EGU start depletes the EES by the amount of $E_\mathrm{G,start}$. Thus, the final SOC $\xi(N)$ of $\Pi_1$ distinctly undercuts the setpoint at the end of the driving cycle in contrast to $\Pi_2$, which results in additional fuel consumption through (54). When start costs are properly incorporated, the number of EGU starts is reduced by 77% from 360 ($\Pi_1$) to 82 ($\Pi_2$). Hence, the fuel consumption is reduced by 2.8% compared to $\Pi_1$ despite the slight deterioration of $\eta_\mathrm{EGU}$.

Second, the aforementioned procedure is repeated for all driving cycles. Figure 14 shows the relative differences of fuel consumption

$$\Delta\tilde{J} = \left(1 - \frac{\tilde{J}^*(\Pi_2)}{\tilde{J}^*(\Pi_1)}\right) \cdot 100 \tag{57}$$

and number of EGU events

$$\Delta n_\sigma = \left(1 - \frac{n_\sigma(\Pi_2)}{n_\sigma(\Pi_1)}\right) \cdot 100 \tag{58}$$

where $(\Pi_1)$ and $(\Pi_2)$ denote affiliation to $\Pi_1$ and $\Pi_2$, respectively. The proper consideration of start costs in $\Pi_2$ reduces fuel consumption by 3.4% in average compared to $\Pi_1$. Thereby, driveability is yet improved since $n_\sigma$ is also reduced by 75% in average. However, frequent changes are still remaining in the EGU state (see Figure 14 bottom, right) which require further improvement of drivetrain activity.

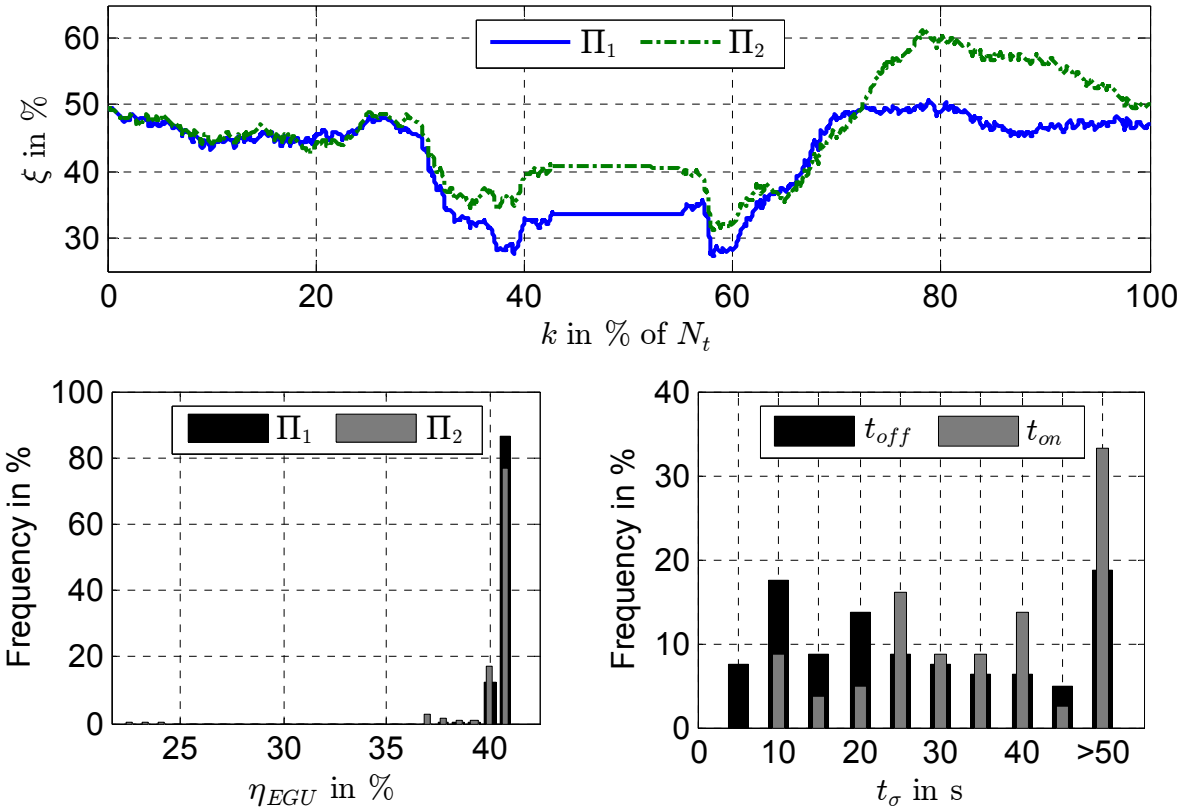


*Figure 13: Impact of $\beta_f$ and $\beta_G$ on state of charge trajectory $\xi$ (top) and EGU efficiency $\eta_{EGU}$ (bottom, left) as well as the time span $t_\sigma$ of all periods with EGU on and off (bottom, right) for a single driving cycle.*

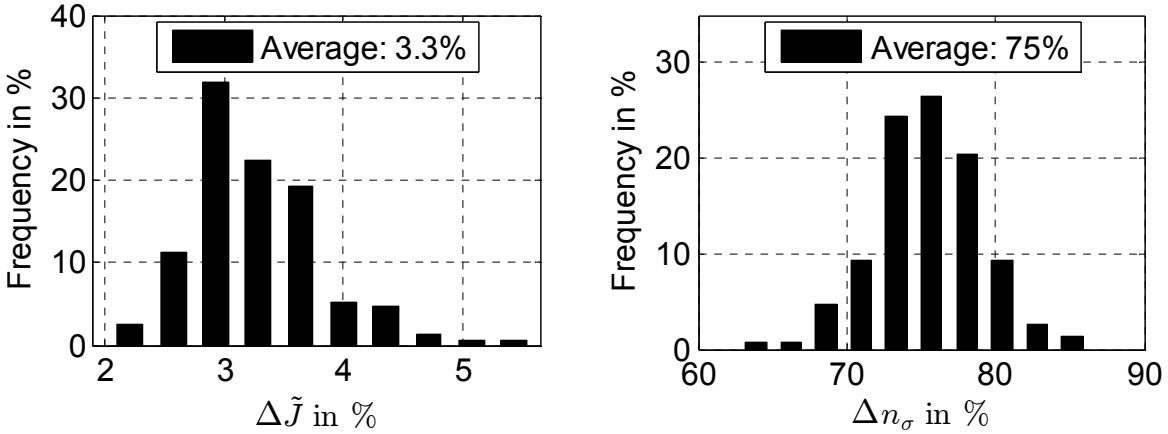


*Figure 14: Histograms of the relative differences of the fuel consumption (left) and the number of EGU events (right). Neglecting $\beta_f$ and $\beta_G$ results in higher fuel consumption and drivetrain activity.*

## 5.3 Sensitivity analysis of the penalty costs for EGU starts

The trade-off between drivetrain activity and fuel consumption is studied by variation of the penalty costs for starting the EGU. Therefore, only $\beta_f$ because variation of $\beta_G$ is not reasonable since it directly affects the EES current and, thus, might result in

immediate violation of the current bounds (23) and charge bounds (24). Note that $\beta_{\mathrm{G}} = E_{\mathrm{G,start}} / t_{\mathrm{start}}$ in contrast to the preceding simulations. Figure 15 illustrates the average values of the number of EGU events $n_\sigma$, the fuel consumption $\tilde{J}^*$ and the minimum EGU off and maximum EGU on time $t_{\mathrm{off}}$ and $t_{\mathrm{on}}$, respectively, of all driving cycles over various values of $\beta_{\mathrm{f}}$. Please keep in mind that the results at $\beta_{\mathrm{f}} = 0$ are not identically equal to those that are depicted in Figure 14 due to $\beta_{\mathrm{G}} = E_{\mathrm{G,start}} / t_{\mathrm{start}}$.

On the one hand, $\tilde{J}^*$ decreases until $\beta_{\mathrm{f}} = E_{\mathrm{f,start}} / t_{\mathrm{start}}$ and approaches its maximum at the largest values of $\beta_{\mathrm{f}}$ because of the following reasons. Firstly, $\eta_{\mathrm{EGU}}$ progressively deteriorates, and secondly, the dissipative losses of the drivetrain increase since the absolute energy throughput of the EES is increased due to the prolonged engagement of the EGU. This means that in periods of low power demand, in which the EGU would be turned off with lower $\beta_{\mathrm{f}}$, the EES is now increasingly charged. On the other hand, $t_{\mathrm{off}}$ and $t_{\mathrm{on}}$ are clearly increased as well with rising $\beta_{\mathrm{f}}$. This means a measurable improvement of drivetrain activity due to the prolonged time duration in one EGU state.

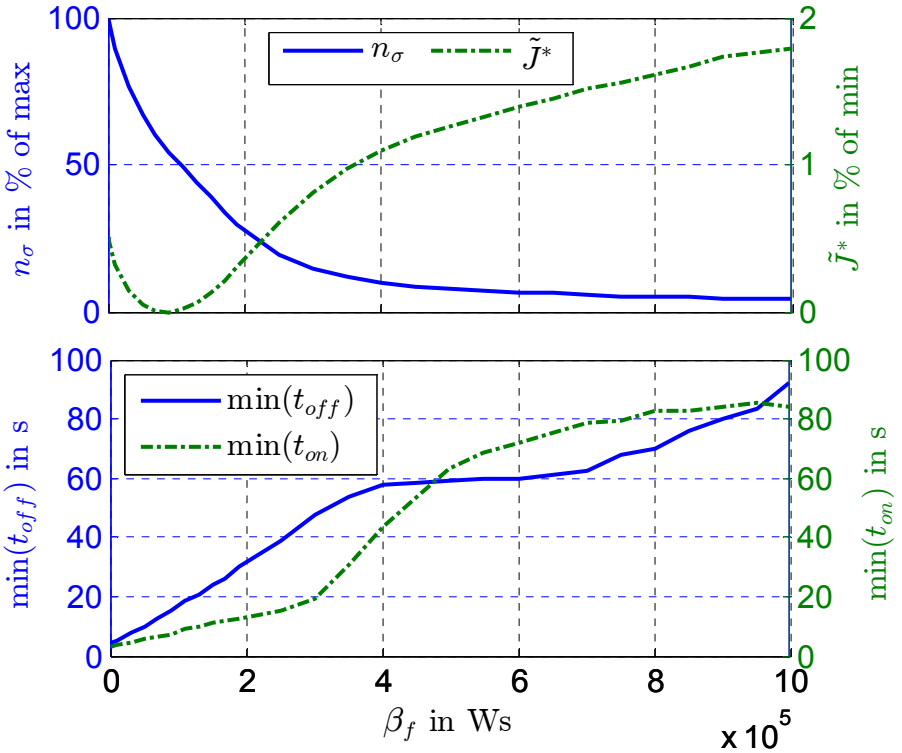


*Figure 15: Normalized average number of EGU starts $n_\sigma$ and fuel consumption $\tilde{J}^*$ (top), minimum EGU off and on time (bottom). The drivetrain activity is clearly reduced with rising penalty costs at the expense of fuel economy.*

## 6. Conclusion and future research

This paper presents a fast and close-to-optimal method for energy management of series hybrid electric vehicles which introduces penalty costs for transitions of discrete states. Moreover, an approach for fuel correction was introduced to account for deviations from final state constraints in terms of battery energy content. This approach uses the equivalence factor to convert battery energy into equivalent fuel consumption with an error of less than 0.2%.
In order to improve driveability, the trade-off between fuel consumption and drivetrain activity has been investigated. Simulations of 151 real-world driving cycles revealed that fuel consumption and drivetrain activity in terms of EGU events will be reduced in average by 3.3% and 75% if engine start costs are properly considered. Furthermore, a sensitivity analysis of the penalty costs has been conducted which shows that drivetrain activity can be significantly lowered at the expense of fuel economy. Although not shown in this paper, the method presented is also applicable to other integer decision variables such as the gear changes.
Future research will focus on extending this method by time constraints on discrete state transitions and investigating their impact on drivetrain activity. A possible next step would be to adopt this method in a model predictive control scheme using ECMS as low level controller. This MPC scheme, which can be used without predictive data, could be the foundation for a simulative study to reveal the potential benefits of using former driving data in MPC of vehicles on fixed routes as a function of different drivetrain configurations.

## Literature

[1] D. Ambühl, O. Sundström, A. Sciarretta, and L. Guzzella, “Explicit optimal control policy and its practical application for hybrid electric powertrains,” *Control Engineering Practice*, vol. 18, no. 12, pp. 1429–1439, 2010.
[2] R. Bellman, *The Theory of Dynamic Programming*. Princeton: Princeton University Press, 1972.
[3] D. P. Bertsekas, *Dynamic programming and optimal control*, 3rd ed. Belmont, Mass: Athena Scientific, 2005-2007.
[4] D. P. Bertsekas, *Approximate dynamic programming*, 4th ed. Belmont, Mass: Athena Scientific, 2012.
[5] S. P. Boyd and L. Vandenberghe, *Convex Optimisation*. Cambridge, UK, New York: Cambridge University Press, 2004.
[6] S. Buerger, B. Lohmann, M. Merz, B. Vogel-Heuser, and M. Hallmannsegger, “Multi-objective optimisation of hybrid electric vehicles considering fuel consumption and dynamic performance,” in *Proc. IEEE Vehicle Power and Propulsion Conference (VPPC)*, 2010, pp. 1–6.
[7] P. Elbert, T. Nuesch, A. Ritter, N. Murgovski, and L. Guzzella, “Engine On/Off Control for the Energy Management of a Serial Hybrid Electric Bus via Convex Optimisation,” *IEEE Trans. Veh. Technol*, vol. 63, no. 8, pp. 3549–3559, 2014.
[8] O. Föllinger, *Optimale Regelung und Steuerung*, 3rd ed, 1994.
[9] J. Froehlich and J. Krumm, “Route Prediction from Trip Observations,” in *Proc. Intelligent Vehicle Initiative (IVI) Technology Advanced Controls & Navigation Systems*, 2008.
[10] L. Guzzella and A. Sciarretta, *Vehicle propulsion systems: Introduction to*

*modeling and optimisation*. Berlin, New York: Springer, 2005.
[11] M. Helbing, S. Uebel, C. Tempelhahn, and B. Bäker, “Bewertender Überblick von Methoden zur Antriebsstrangsteuerung von Hybrid-Elektrofahrzeugen,” *ATZ - Automobiltechnische Zeitschrift*, pp. 67–71, 2015.
[12] B. de Jager, T. van Keulen, and J. Kessels, *Optimal Control of Hybrid Vehicles*. London: Springer, 2013.
[13] L. Johannesson, “Predictive Control of Hybrid Electric Vehicles on Prescribed Routes,” Dissertation, Department of Signals and Systems, Chalmers University of Technology, Göteborg, Sweden, 2009.
[14] T. v. Keulen, J. Gillot, B. d. Jager, and M. Steinbuch, “Solution for state constrained optimal control problems applied to power split control for hybrid vehicles,” *Automatica*, vol. 50, no. 1, pp. 187–192, http://www.sciencedirect.com/science/article/pii/S000510981300472X, 2014.
[15] S. Kutter, “Eine prädiktive und optimierungsbasierte Betriebsstrategie für autarke und extern nachladbare Hybridfahrzeuge,” Dissertation, Institut für Automobiltechnik, Technische Universität Dresden, Dresden, 2012.
[16] S. Kutter and B. Baker, “An iterative algorithm for the global optimal predictive control of hybrid electric vehicles,” in *Proc. IEEE Vehicle Power and Propulsion Conference (VPPC)*, 2011, pp. 1–6.
[17] A. A. Malikopoulos, “Supervisory Power Management Control Algorithms for Hybrid Electric Vehicles: A Survey,” IEEE Trans. Intell. Transport. Syst, vol. 15, no. 5, pp. 1869–1885, 2014.
[18] N. Murgovski, L. M. Johannesson, and J. Sjoberg, “Engine On/Off Control for Dimensioning Hybrid Electric Powertrains via Convex Optimisation,” *IEEE Trans. Veh. Technol*, vol. 62, no. 7, pp. 2949–2962, 2013.
[19] V. D. Ngo, “Gear Shift Strategies for Automotive Transmissions,” Dissertation, Eindhoven University of Technology, Eindhoven, 2012.
[20] V. D. Ngo, “Optimal Control of the Gearshift Command for Hybrid Electric Vehicles,” in *Proc. IEEE Transactions on Vehicular Technology, vol. 61, no. 8*, 2012, pp. 3531–3543.
[21] T. Nüesch, P. Elbert, M. Flankl, C. Onder, and L. Guzzella, “Convex Optimisation for the Energy Management of Hybrid Electric Vehicles Considering Engine Start and Gearshift Costs,” Energies, vol. 7, no. 2, p. 834, http://www.mdpi.com/1996-1073/7/2/834, 2014.
[22] D. F. Opila, D. Aswani, R. McGee, J. A. Cook, and J. W. Grizzle, “Incorporating Driveability Metrics into Optimal Energy Management Strategies for Hybrid Vehicles,” *Proc. 47th IEEE Conference on Decision and Control*, 2008.
[23] G. Paganelli, T. M. Guerra, S. Delprat, J.-J. Santin, M. Delhom, and E. Combes, “Simulation and assessment of power control strategies for a parallel hybrid car,” Proceedings of the Institution of Mechanical Engineers, Part D: Journal of Automobile Engineering, vol. 214, no. 7, pp. 705–717, 2000.
[24] A. Panday and H. O. Bansal, “A Review of Optimal Energy Management Strategies for Hybrid Electric Vehicle,” *International Journal of Vehicular Technology*, vol. 2014, p. 19, http://dx.doi.org/10.1155/2014/160510, 2014.
[25] P. Pisu, K. Koprubasi, and G. Rizzoni, “Energy Management and Driveability Control Problems for Hybrid Electric Vehicles,” in *Proc. 44th IEEE Conference on Decision and Control*, 2005, pp. 1824–1830.
[26] F. R. Salmasi, “Control Strategies for Hybrid Electric Vehicles: Evolution, Classification, Comparison, and Future Trends,” *IEEE Trans. Veh. Technol*, vol. 56, no. 5, pp. 2393–2404, 2007.

[27] A. Sciarretta, M. Back, and L. Guzzella, “Optimal control of parallel hybrid electric vehicles,” *IEEE Transactions on Control Systems Technology*, vol. 12, no. 3, pp. 352–363, 2004.
[28] A. Sciarretta and L. Guzzella, “Control of Hybrid Electric Vehicles: Optimal Energy-Management Strategies,” *IEEE Controll Systems Magazine*, pp. 60–70, 2007.
[29] L. Serrao, “A Comperative Analysis of Energy Management Strategies for Hybrid Electric Vehicles,” Dissertation, The Ohio State University, 2009.
[30] V. S. Tiwari, A. Arya, and S. Chaturvedi, “Route prediction using trip observations and map matching,” in *Proc. 3rd IEEE International Advanced Computing Conference (IACC 2013)*, 2013, pp. 583–587.
[31] S. Uebel, C. Tempelhahn, M. Liebers, S. Kutter, and B. Bäker, “Anwendung der Variationsrechnung für Steuerungsaufgaben im Kraftfahrzeug,” *at – Automatisierungstechnik*, vol. 62, no. 4, 2014.
[32] F. Vidal-Naquet and G. Zito, “Adapted optimal energy management strategy for driveability,” in Proc. IEEE Vehicle Power and Propulsion Conference (VPPC), 2012, pp. 358–363.
[33] X. Wei, P. Pisu, G. Rizzoni, and S. Yurkovich, “Dynamic Modeling of a Hybrid Electric Drivetrain for Fuel Economy, Performance and Driveability Evaluations,” in *Proc. of ASME International Mechanical Engineering Congress*, 2003, pp. 1–8.
[34] S. G. Wirasingha and A. Emadi, “Classification and Review of Control Strategies for Plug-In Hybrid Electric Vehicles,” *IEEE Trans. Veh. Technol*, vol. 60, no. 1, pp. 111–122, 2011.
[35] Z. Yuan, L. Teng, S. Fengchun, and H. Peng, “Comparative Study of Dynamic Programming and Pontryagin’s Minimum Principle on Energy Management for a Parallel Hybrid Electric Vehicle,” *Energies*, vol. 6, no. 4, pp. 2305–2318, 2013.